Journal of Neuropathology & Experimental Neurology, 2024, 1–13
https://doi.org/10.1093/jnen/nlae079
Original Article

OXFORD

Cytoplasmic vacuolization and ectopic formation of perineuronal nets are characteristic pathologies of cytomegalic neurons in tuberous sclerosis

Alexander A. Sosunov, MD, PhD[1], Guy McKhann, II, MD[1], Guomei Tang, PhD[2], James E. Goldman, MD, PhD[3,4,*]

[1]Department of Neurological Surgery, Columbia University Irving Medical Center, New York, NY, United States
[2]Department of Neurology, Columbia University Irving Medical Center, New York, NY, United States
[3]Department of Pathology and Cell Biology, Columbia University Irving Medical Center, New York, NY, United States
[4]The Taub Institute for Research on Alzheimer's Disease and the Aging Brain, Columbia University Irving Medical Center, New York, NY, United States

*Send correspondence to: James E. Goldman, MD, PhD, Department of Pathology and Cell Biology, The Taub Institute for Research on Alzheimer's Disease and the Aging Brain, Columbia University Irving Medical Center, 630 West 168th St, New York, NY 10032, United States; E-mail: jeg5@cumc.columbia.edu

ABSTRACT

Cytomegalic neurons, characterized by increased size and a hyperactive mechanistic target of rapamycin complex 1 (mTORC1), are pathognomonic for tuberous sclerosis complex (TSC). To model these neurons, we recently generated a murine *Tsc1* conditional knockout model in which *Tsc1* deletion in late embryonic radial glia results in neuronal hypertrophy of a subset of isocortical pyramidal neurons. In the current study, we compared the cellular pathology of these cytomegalic neurons to those of the enlarged neurons in human cortical tubers. Neurons from the mice showed unique features, such as cytoplasmic vacuoles associated with Golgi complexes and the ectopic formation of perineuronal nets (PNNs), a feature of inhibitory neurons, rarely present in excitatory cortical neurons. The membranes of these vacuoles were enriched for the plasma membrane proteins CD44, KCC2, and Na+/K+ ATPase, suggesting deficits in Golgi membrane trafficking. These aberrant features in the mouse appeared only after the onset of seizures, probably due to the prolonged seizure activity in the context of constitutive mTORC1 activation. Similar PNNs and cytoplasmic vacuoles were present in the cytomegalic neurons of human cortical tubers. Our findings reveal novel pathological features of Golgi complexes and PNNs in the cytomegalic neurons in TSC.

KEYWORDS: CD44; cytomegalic neurons; Golgi complex; KCC2; Na+/K+ ATPase; perineuronal nets; tuberous sclerosis

INTRODUCTION

Tuberous sclerosis complex (TSC) is a genetic disorder due to mutations in *TSC1* or *TSC2* genes, which lead to uncontrolled hyperactivity of the mechanistic target of rapamycin (mTOR). Multiple systems are involved in the disease and patients often suffer from severe, intractable seizures, cognitive decline, and autistic behavior.[1,2] Brain abnormalities include canonical focal lesions such as cortical tubers, subependymal glial nodules, and subependymal giant cell astrocytomas (SEGA), as well as recently described widespread, diffuse alterations in the form of microtubers and sentinel giant cells.[3–5] The characteristic morphological features of cortical tubers are dysmorphic, cytomegalic neurons and giant cells, both of large size due to a constitutively active mTOR cascade leading to increased protein synthesis.[6] Several murine models based on the conditional or inducible deletion of *Tsc1* or *Tsc2* recapitulate TSC, including the appearance of enlarged neurons.[7–12] The emergence of enlarged neurons is also characteristic of mTOR activation by upstream activators such as PI3K and PTEN.[13–16]

Recently, we described a novel murine model of *Tsc1* deletion under the *mGFAP-Cre* promoter.[17] The Cre-based recombination occurred in early neuronal precursors (starting from E17 in radial glia), and in adult mice the majority of astrocytes and some neurons were recombinant. One striking feature was the appearance of highly enlarged pyramidal neurons in the isocortex (named "cytomegalic pyramidal neurons" or "CPNs"), about half of them reaching more than 40 μm in diameter by 3.5 months (M) of age. CPNs had high levels of phosphorylated-S6-ribosomal protein (pS6), a reliable marker of mTOR activity. All CPNs were glutamatergic principal neurons, expressing AMPA and NMDA receptors, and showed increased glutamatergic synaptic transmission and an increased propensity to seizure-like activity.

Here, we present a detailed analysis of CPNs after the onset of seizures and describe novel pathological features, including

cytoplasmic vacuoles that retained plasma membrane proteins, including ion transporters, and the presence of perineuronal nets (PNNs) around the CPNs. The cytomegalic neurons in the cortical tubers of human TSC also have these abnormal features.

METHODS

Mouse strains

Tsc1$^{flox/flox}$(*Tsc1*^{tm1Djl}/J)(https://www.jax.org/strain/005680), *mGFAP-Cre* (B6.Cg-Tg(Gfap-cre)73.12Mvs/J (http://jaxmice.jax.org/strain/012886), and Ai9 (B6.*Cg-Gt(ROSA)26Sor*$^{tm9(CAG-tdTomato)Hze}$/J, (https://www.jax.org/strain/007909) mice were obtained from The Jackson Laboratory. The breeding strategy with *mGFAP-Cre*, *TSC1*$^{flox/flox}$, and Ai9 was recently presented, giving us the *Tsc1mGfap-CreCKO: Ai9*+mice (known as *Tsc1CKO*).[17] All mouse experimental procedures were reviewed and approved by the Columbia University Medical Center Institutional Animal Care and Use Committee.

Human tissue

Specimens including cortical tubers ($n = 16$) were obtained from TSC patients with medically refractory epilepsy who were undergoing epilepsy surgical resection. The mean age of the 16 patients was 9.8 ± 1.5 years (range: 2.5-23 years), with 9 females and 7 males. The epileptogenicity of the resected tubers and perituberal tissue was established during invasive subdural intracranial monitoring of patients, as previously described.[18] All patient protocols were approved by the Institutional Review Board of Columbia University Medical Center.

All investigations were carried out following the rules of the Declaration of Helsinki of 1975. Human brain tissues from patient brain biopsies, which were diagnosed based on accepted neuropathological criteria, were obtained from the Department of Pathology and Cell Biology of Columbia University. All surgeries were performed with the consent of the patients, and studies from biopsy tissues are provided without any patient identifying information. The Institutional Review Board of Columbia University has determined that clinicopathologic studies on de-identified tissue samples are exempt from Human Subject Research according to Exemption 45 CFR 46.104(d).[2]

Histology and immunohistochemistry

Mice were anaesthetized with isoflurane before intracardiac perfusion with cold phosphate buffered saline (PBS) followed by cold 4% paraformaldehyde (PFA). Brains were removed and kept in the fixative for 12-16 h at 4°C. Forty micrometer coronal sections were prepared with a vibratome (Leica VT1000S) and stored in cryoprotectant solution at −20°C before use.

Surgical specimens were fixed in PFA for 14-18 h at 4°C. Forty micrometer sections were prepared with a vibratome (Leica VT1000S) and stored in cryoprotectant solution at −20°C. Standard procedure Nissl staining with Cresyl violet was used for routine analysis of tissue. Some samples were embedded in paraffin and 4 µm sections were stained with hematoxylin and eosin.

Primary antibodies used in the study are presented in Table 1. Secondary antibodies included: anti-mouse Alexa Fluor 488, 594, 647; anti-rabbit Alexa Fluor 488, 594, 647; anti-rat Alexa Fluor 488 and 594; all from goat or donkey (1:300, ThermoFisher Scientific, Waltham, MA, United States).

For immunofluorescence, after blocking with 10% normal goat (or donkey) serum (30 min) at room temperature free-floating sections were incubated overnight in a mixture of primary antibodies raised in different species (4°C). For visualization, Alexa Fluor-conjugated secondary antibodies were applied for 1 h at room temperature. For nuclear staining, Fluorescent Nissl reagent (NeuroTrace 640/660 deep-red, 1:150, Molecular Probes, Eugene, OR, United States) or DAPI (5 µg/mL; D9542, Sigma-Aldrich, St Louis, MO, United States) was added to secondary antibodies. Paraffin sections and vibratome sections were treated with Antigen Unmasking Solution (# H-3300, Vector Laboratories, Burlingame, CA, United States) according to manufacturer's recommendations before blocking with serum. Blocking serum, primary, secondary antibodies were applied in 0.2% Triton X-100 in PBS. Sections for fluorescent microscopy were mounted on slides in Vectashield (Vector Laboratories). To control for the specificity of immunostaining, primary antibodies were omitted and substituted with appropriate normal serum. Slides were viewed using a Nikon A1R MP confocal microscope. 3D reconstructions were generated from stacks of images with confocal microscope software NIS-Elements.

Electron microscopy

For regular transmission electron microscopy (EM) mice were anaesthetized with isoflurane before intracardiac perfusion with cold PBS followed by cold 2% glutaraldehyde + 2% PFA. Brains were kept in fixative for 12-16 h at 4°C and small pieces of upper neocortices were cut, and after washing were post-fixed in 2% osmium tetroxide in 0.2 PBS for 2 h at 4°C, dehydrated and embedded in Epon-Araldite (Electron Microscopy Sciences, Hatfield, PA, United States). Vibratome slices for EM were additionally fixed in 2.5% glutaraldehyde in PBS (2 h at 4°C), postfixed in 2% osmium tetroxide in 0.2 PBS (2 h at 4°C), dehydrated, and flat-embedded in Epon-Araldite on ACLAR Embedding Film (Ted Pella, Inc., Redding, CA, United States). Areas of interest were identified under the light microscope, cut from sections, and glued onto resin blocks. Ultrathin sections were cut with a Reichert Ultracut E, stained with uranyl acetate and lead citrate, and examined with a JEOL 1200 electron microscope.

Quantification of cell numbers

Numbers of neurons of interest were calculated in at least 5 coronal sections from one brain at different rostro-caudal levels; 5-6 mice were used for each measured variable.

Statistical analysis

Data are expressed as mean ± SEM. Continuous parameters were analyzed with the Student *t*-test or with one-way ANOVA. $P < .05$ was considered significant.

Table 1. Antibodies used in this study.

CD44	Rat monoclonal	Calbiochem, San Diego, CA	#217594	1:200
ERGIC-53	Mouse monoclonal	Santa Cruz Biotechnology, Santa Cruz, CA	sc-365158	1:100
K+/Cl- Cotransporter (KCC2)	Rabbit polyclonal	EMD Millipore Corp.Temecula, CA	#07-432	1:500
K+/Cl- Cotransporter (KCC2)	Mouse monoclonal	Millipore	MABN88	1:200
MAP2	Rabbit polyclonal	Millipore	AB5622	1:500
Na+/K+-ATPase α1	Rabbit polyclonal	Millipore	#06-520	1:300
Pan-neuronal neurofilament marker (SMI 311)	Mouse monoclonal	Covance, Emeryville, CA	SMI-311R	1:500
NeuN	Mouse monoclonal	Millipore	MAB377	1:100
Phospho-S6 ribosomal protein (Ser 235/236)	Rabbit monoclonal	Cell Signaling Technology, Inc, Boston, MA	#4857	1:200
TGN46	Rabbit polyclonal	ThermoFisher Scientific, Fair Lawn, NJ	PA5-23068	1:200
TGN38	Rabbit polyclonal	Novus Biologicals,Centennial, CO	NBP1-03495SS	1:100
Calreticulin	Rabbit polyclonal	Cell Signaling	#12238	1:200
GRP78 BiP	Rabbit polyclonal	Abcam	Ab21685	1:500
EAA1	Rabbit polyclonal	ThermoFisher Scientific	PA5-29013	1:250
Ubiquitin	Rabbit polyclonal	Millipore	AB1690	1:500

RESULTS

In the *Tsc1CKO* mice, we examined CPNs with immunohistochemistry and EM and observed a number of unusual features. The abnormalities were observed only in mice with seizures at the age of 3 M and older, ie, when CPNs have reached a large size and are easily differentiated from normal-sized neurons. A Nissl stain of a non-mutant mouse isocortex compared to that of the *Tsc1CKO* mouse reveals the enlarged neurons in the mutant (Figure 1A, A', and B). Note that in the *Tsc1CKO* mouse there are normal-sized neurons, some of which are non-recombinant, but others of which are recombinant, as determined by the staining with pS6 (Figure 1B).

Formation of vacuoles in the cytoplasm is a characteristic CPN abnormality subsequent to seizures

One of the notable pathologic findings in the mouse CPNs was the presence of cytoplasmic vacuoles. Because they were single membrane-bound vacuoles, we chose to use antibodies to several plasma membrane proteins to identify some of their constituents. We found 3 membrane proteins associated with the vacuoles: CD44, a receptor for hyaluronan and other matrix molecules that is found in astrocytes in the human CNS[19] and in astrocytes and cerebellar granule cells but not cortical neurons in the adult mouse CNS[20,21]; KCC2, a potassium-chloride cotransporter controlling intracellular Cl^- concentration that is widely expressed in the plasma membrane of cortical neurons (Figure 3A, A1, and A'); and Na+/K+ ATPase α-1, a plasma membrane ion pump critical for neuronal excitability (Figure 3B and C).

The CD44 immunoreactivity in CPNs showed 2 different patterns. In some CPNs, CD44 outlined the plasma membrane, including dendritic spines and the thin spine-like protrusions from the perikaryon (Figure 2A and B), whereas in other CPNs, CD44 showed weak or no staining of the plasma membrane but a prominent staining of cytoplasmic, vacuole-like profiles, producing in some neurons a honeycomb-like pattern (Figure 2C and D). The vacuole membranes in many CPNs were also positive for KCC2 (Figure 3A). In CPNs with vacuoles that were immunopositive for KCC2, ∼30% of the vacuoles (37 of 96) were also stained for CD44. Immunoreactivity for Na+/K+ ATPase α-1 was present in vacuole membranes (Figure 3B) and in small cytoplasmic foci in some neurons, where it was colocalized with CD44 (Figure 3C and C1). Note that some of the vacuoles looked empty (Figure 2C' and D) where the antibody reacted only with the peripheral membrane, while others looked partly or completely full of the immunostain (Figure 2C' and 3A and B). There are two reasons for this variability of the staining. First, the images through a Z stack of the confocal pictures often showed a "filled" vacuole at one level and an "empty" vacuole at another level (see Supplementary Data movies showing animations through the Z stacks). Second, as seen below in the EM studies, some vacuoles were filled with cytoplasmic protrusions, the membranes of which are continuous with the vacuolar membrane, while others are empty. Notably, the soluble reporter used for the identification of recombinant neurons, tdTomato, was not observed inside the vacuoles, demonstrating a membrane barrier between cytoplasm and the interior of the vacuoles (not shown).

Under the EM (Figure 4), the vacuoles in the CPNs were separated from the cytoplasm by a single membrane (Figure 4B1, B2, C1', C1'', and D1). Thin cytoplasmic protrusions containing common organelles, such as mitochondria, vesicles, and ribosomes, all of which displayed a normal ultrastructure, projected into the vacuoles. These "intra-vacuolar" cytoplasmic inclusions were outlined by single membranes and occupied either much of a vacuole (Figure 4C and D) or only part of a vacuole (Figure 4B). Such ultrastructure

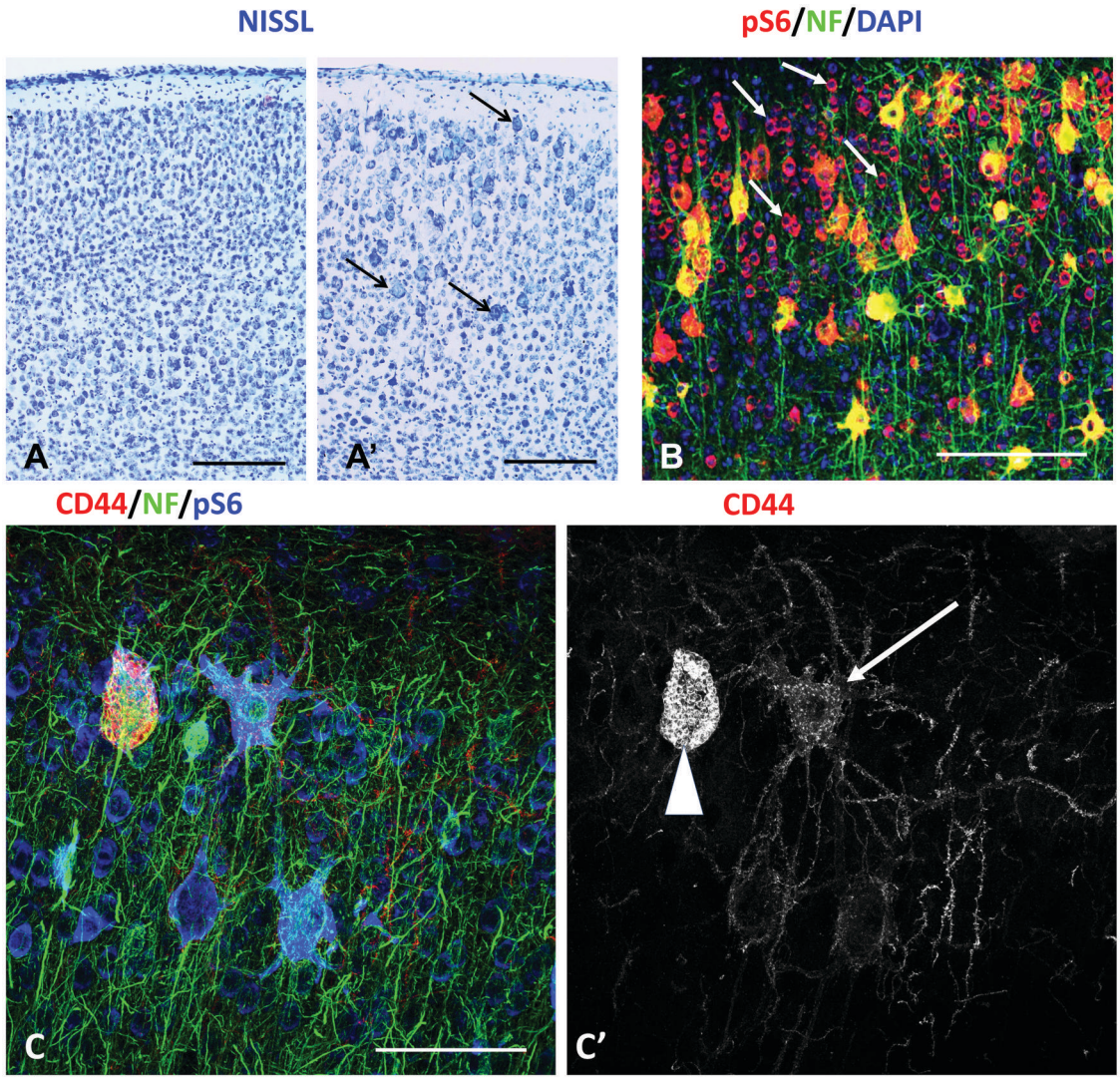

Figure 1. Aberrant features of cytomegalic pyramidal neurons (CPNs). (A, A') Neocortex in *Tsc1CKO* mice (A') differ from control (A) by the presence of CPNs (arrows, only some marked) that predominated in upper cortical layers. Nissl staining of vibratome sections of 6M mice. (B) CPNs are characterized by large size and high levels of neurofilaments (NF) and pS6 (note yellow color of large neurons indicating a mixture of green (NF) and red (pS6). Note that many neurons of normal size express pS6 (some are marked with arrows). (C) Two typical patterns of CD44 expression in CPNs: (1) CD44 accumulates in plasma membrane including cell bodies and processes (arrow in C') and (2) CD44 is found predominantly in the membranes of intracytoplasmic vacuoles (arrowheads in C'). Immunostains on 3M *Tsc1CKO* mice. Confocal microscopy. Scale bars: A, A'= 110 μm, B = 85 μm, C = 45 μm.

explains why at the level of confocal microscopy, some vacuoles looked partly empty whereas others appeared to contain immunopositive material, such as CD44 (Figure 2A and B) or KCC2 and Na+/K+ ATPase (Figure 3A and B). We noted that small vacuole-like profiles were often observed in close proximity to Golgi complexes with distended cisterns (Figure 4E and F).

To assess the origin of these vacuoles, we examined immunoreactivity for several proteins that might be related to their formation. We did not find evidence that p62 or ubiquitin, markers of products targeted to autophagy, (although not fully specific for autophagy), were associated with the vacuoles. Furthermore, no vacuole was enclosed by a double membrane typical for autophagic vacuoles.[22] Thus, it seems unlikely that the vesicles are autophagic vacuoles.

Markers of endoplasmic reticulum (ER), calreticulin and Bip, did not show colocalization with vacuoles. EEA1, an endosomal marker, was observed as small dot-like puncta in the cytoplasm and did not aggregate in the walls or content of vacuoles. Of note, distended cisterns of ER were not observed by EM in the vicinity of or in contact with the vacuoles.

Proteins of the Golgi complex, ERGIC (marker of ER-Golgi compartment) and TGN38 (marker of the trans-Golgi network), were not found in the walls of vacuoles (Figure 5E and F), but were colocalized with CD44 and/or KCC2 in small profiles of Golgi (Figure 5A–D).

Note in Figure 5D' (part of Figure 5D that represents only a few optical slices), there is a small vacuole with a peripheral localization of KCC2 in the wall (in green), and a Golgi marker (in red) and CD44 (in blue) in the central part. An

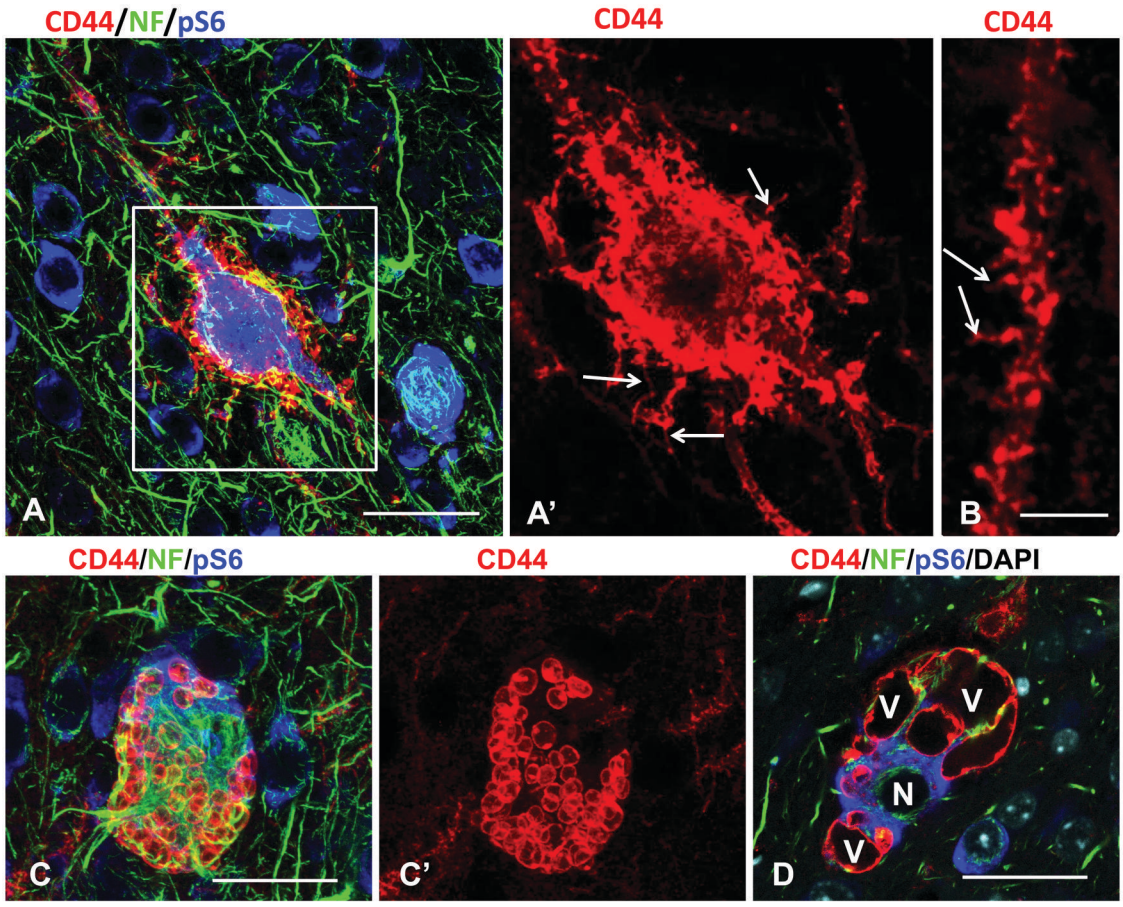

Figure 2. Two characteristic types of CD44 localization in CPNs. (A) CD44 accumulates in the plasma membrane, including thin processes from the perikaryon (A', arrows) and dendritic spines (B, arrows). (C) CD44 is found predominantly in the membranes and content of intracytoplasmic vacuoles. Note that vacuoles in the neuron in (C) are of similar size and differ in the intravacuole volume occupied by immunopositive material. (D) One optical section through a CPN filled with vacuoles [V] of different sizes. Note that large vacuoles are devoid of immunostained content. N-nucleus. 3M *Tsc1CKO* mice. Confocal microscopy. Scale bars: A = 50 μm, B = 15 μm, C = 20 μm, D = 45 μm.

additional movie file shows animation that progresses through the Z-stack of this image in more detail (Supplementary File S1 and Supplementary Legends File). Vacuoles in some neurons contained CD44+ material (Figure 5E and its boxed area in Figure 5E'). An additional movie file showing animation that progresses through the Z-stack of Figure 5E' is presented in more detail (Supplementary File S2 and Supplementary Legends File). Some vacuoles contained small foci of Golgi material (TGN38) and others contained larger sized ovals of KCC2 (Figure 5F and its boxed area in Figure 5F'). An additional movie file shows animation that progresses through the Z-stack of Figure 5F' in more detail (Supplementary File S3 and Supplementary Legends File.

CPNs are abnormally surrounded by PNNs

Many CPNs were surrounded by PNNs, a specific organization of perineuronal extracellular matrix identified with Wisteria floribunda agglutinin (WFA) (Figure 6A). We also found WFA staining in the cytoplasmic vacuoles; in some vacuoles, WFA was colocalized with KCC2 (Figure 6B). WFA was observed in Golgi in a "trans" position in contact with ERGIC in the "cis" position (Figure 5B). These nets are a typical feature of inhibitory but not of excitatory neurons in the isocortex.[23] The non-recombinant pyramidal neurons and the normal-sized recombinant pyramidal neurons did not have PNNs.

Cytomegalic neurons in human cortical tubers contain vacuoles and PNNs similar to those in mice

Cytomegalic neurons were easily identified in cortical tubers by their large size, the appearance of large Nissl bodies, and a nucleus with prominent nucleolus. They displayed high immunoreactivity for neuronal markers such as neurofilaments (NF) (Figure 7A and D), MAP2, and pS6 (not shown). Some of the cytomegalic neurons were surrounded by PNNs (Figure 7A). None of the small neurons with PNNs, which are likely parvalbumin inhibitory neurons ($n = 121$), reached the size of cytomegalic neurons.

In the cytomegalic neurons that contained cytoplasmic vacuoles (Figure 7B), the vacuoles were immunoreactive for

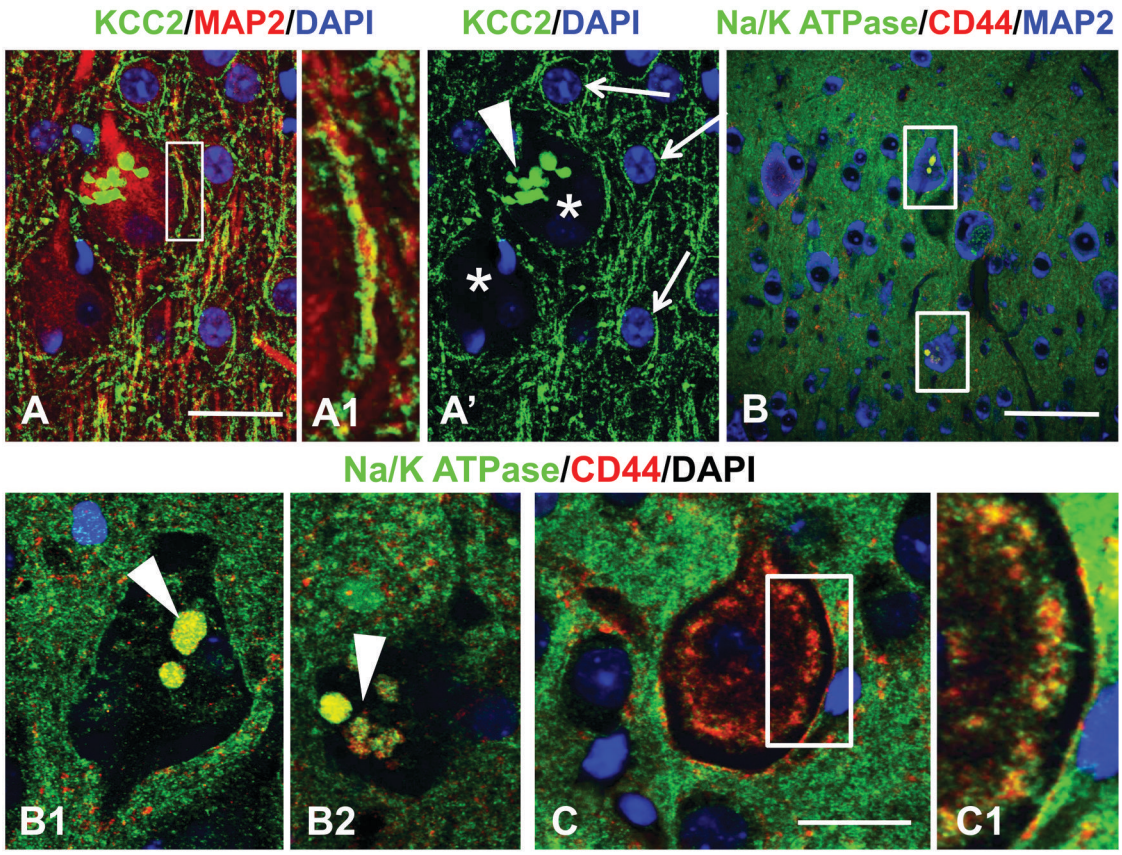

Figure 3. Expression of plasma membrane proteins KCC2 and Na+/K+ ATPase in intraneuronal vacuoles in CPNs. (A) The vacuoles immunostained for KCC2 were found in one of two neighboring CPNs (both are marked with asterisks in A'). (A1) Enlarged boxed area in (A) showing a MAP2+/KCC2+ dendrite passing near to and along the CPN. Note that these CPNs (asterisks) do not have KCC2 staining at their plasma membranes, in contrast to the neighboring normal sized neurons (arrows). (B) CPNs with vacuoles immunopositive for Na+/K+ ATPase. Note in (B1) and (B2) that the vacuoles in the neurons shown in (B) are also immunopositive for CD44 (vacuoles are yellow due to the combination of green and red colors). (C) Small foci that may correspond to Golgi are double stained for CD44 and Na/K ATPase (indicated by the yellow color). (C1) Enlarged boxed area in (C) shows small yellow foci corresponding to colocalized CD44 and Na/K ATPase. 3 M *Tsc1CKO* mice. Confocal microscopy. Scale bars: A = 25 μm, B = 65 μm, C = 35 μm.

KCC2 and Na+/K+ ATPase, similar to those in the *Tsc1CKO* mice, but not CD44 (Figure 7C and D). We used several markers of the Golgi complex and, (as in *Tsc1CKO* mice), did not observe staining of vacuole membranes. Similar also to mice, KCC2 was colocalized with TGN46 (a marker of the "trans" Golgi compartment) in small profiles of Golgi (Figure 7E and E1). An additional movie file shows animation that progresses through the Z-stack shown in 7E1 (Supplementary File S4 and Supplementary Legends File). Ultrastructurally, the vacuoles in cytomegalic neurons appeared similar in composition and morphology to those in the *Tsc1CKO* mice, including the protrusions of membrane bound cytoplasm into the vacuoles (Figure 8). We did not notice other pathological ultrastructural changes in neurons with vacuoles.

DISCUSSION

In the *Tsc1CKO* mice, CPNs differ in many ways from the non-recombinant and normal-sized recombinant neurons. Some differences are primarily quantitative, such as cellular hypertrophy or an increase in the number of processes and dendritic spines. These appear early, in 1 M mice, and are present in mice with and without seizures.[17] Other differences, such as the appearance of vacuoles, are qualitative and represent pathological alterations. They were observed only in mice with seizures, usually at 3 M of age and older. We consider that the first changes are cell-autonomous and direct results of *Tsc1* deletion, whereas the second changes are network-dependent and triggered synergistically by seizures and *Tsc1* deletion.

Possible origins of cytoplasmic vacuoles

One of the notable abnormal features of CPNs was the appearance of cytoplasmic vacuoles. We consider that these vacuoles may originate from Golgi cisterns. First, as seen with EM, many cisterns of Golgi were distended and small vacuoles filled with invaginated pieces of cytoplasm were located in direct contact with the Golgi. Second, all three markers identified in vacuoles (CD44, KCC2, and Na+/K+-ATPase) were colocalized with Golgi markers in small cytoplasmic foci.

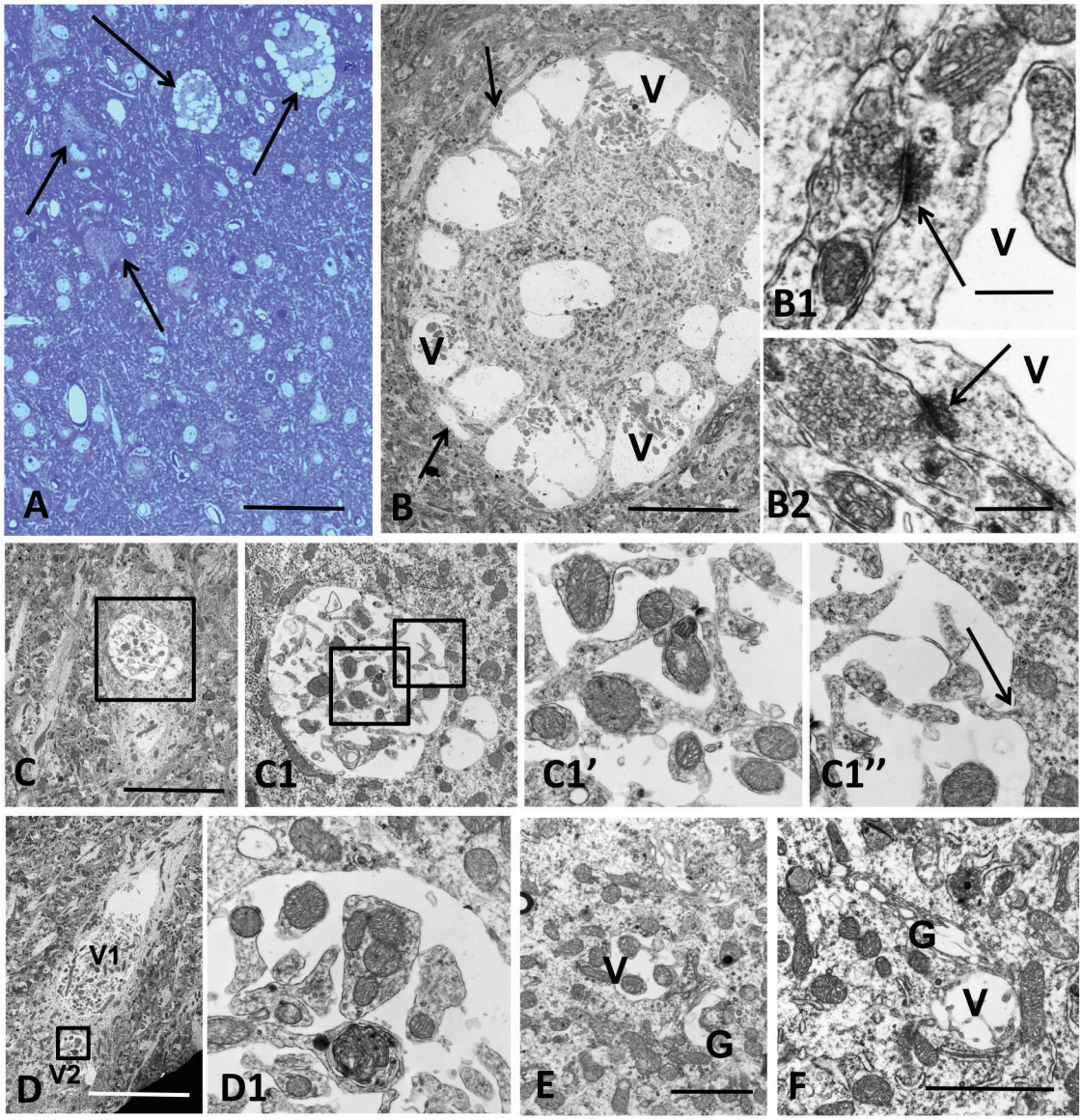

Figure 4. Ultrastructure of neurons with vacuoles in *Tsc1CKO* mice. (A) Semi-thin section stained with toluidine blue. Cytomegalic pyramidal neurons (CPNs) (arrows) contain vacuoles while other neurons do not. (B) A neuron with vacuoles [V] has many axo-somatic synapses (arrows in B1 and B2) (V-vacuole, arrows indicate active synaptic zones). (C) A neuron with two large vacuoles (the upper is boxed and shown enlarged in C1, C1', and C1''). The vacuole is filled with thin cytoplasmic "processes", many containing mitochondria with normal ultrastructure. Arrow in (C1'') indicates the point at which this process is continuous with the perivacuolar cytoplasm. (D) Large vacuoles (V1 and V2) filled with thin cytoplasmic protrusions, many of which contain mitochondria (D1, enlarged boxed area in D). (E, F) Small profiles of vacuoles [V] in close contacts with Golgi (G). 3 M (A, B) and 4 M (C-F) *Tsc1CKO* mice. Scale bars: A = 85 μm, B = 8 μm, C, D = 40 μm, E, F = 15 μm.

This might be the beginning of vacuolar growth although they may represent small Golgi fragments. Third, we did not find evidence by immunohistochemistry and EM that vacuoles originate from ER or are related to autophagy. A schematic presentation of the proposed structural reconstruction of Golgi with the appearance of vacuoles is presented in Figure 9.

We do not exclude other possible membrane systems from which these vacuoles may originate. These include autophagosomes and lysosomes, both single membrane-bound structures within cells, although the vacuoles do not appear to contain cellular debris. They do contain what seem to be isolated membrane-bound pieces of cytoplasm that we interpret to be parts of the cytoplasmic projections into the vacuoles because the organelles appear normal and some of these isolated pieces are connected by thin cytoplasmic bridges to the adjacent neuronal cytoplasm.

The lack of plasma membrane staining with KCC2 in some of the vacuolated neurons seems consonant with reports of seizures being associated with a lack of plasma membrane KCC2.[24,25] Indeed, *KCC2* downregulation itself can cause seizures.[26] This lack of plasma membrane KCC2 could result

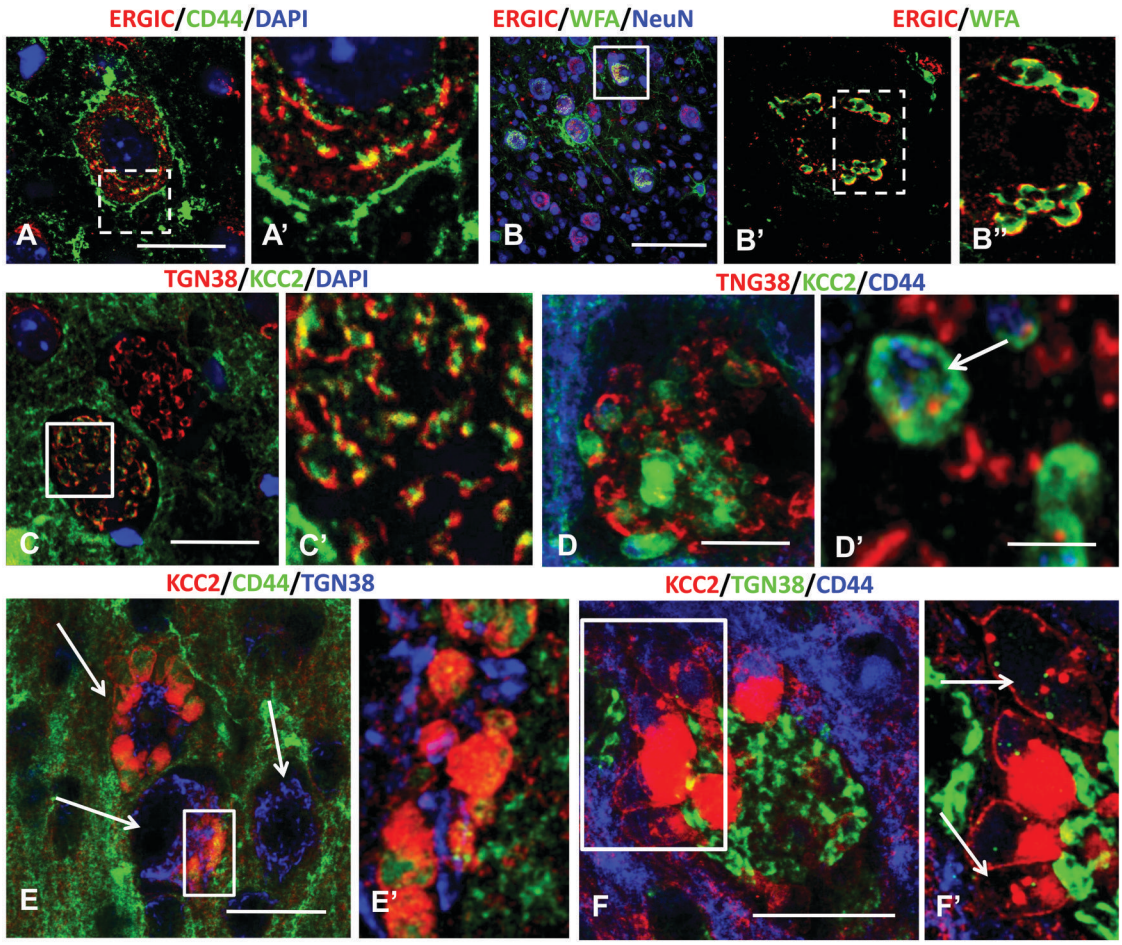

Figure 5. Colocalization of CD44, Wisteria floribunda agglutinin (WFA), and KCC2 with markers of Golgi complex ERGIC (cis side) (A, B) and TGN38 (trans side) (C, D). (A, B) Note that CD44 and WFA take a trans Golgi position near ERGIC located on the cis side. In (C) and (D) note that TGN38 is partly colocalized with KCC2 (indicated by the yellow color). The small vacuole indicated with the arrow in (D') where the vacuole wall is composed of KCC2 and partly of TGN38, whereas CD44 is found in the central part of the vacuole. For a 3D reconstruction of this image along the Z axis (Supplementary File S1 and Supplementary Legends File). (E) Three cytomegalic pyramidal neurons (CPNs) (arrows), two of which contain KCC2+ vacuoles. The boxed area in E is shown enlarged in (E') and see in in the Z axis animation (Supplementary File S2 and Supplementary Legends File). The colocalization of KCC2 and TGN 38 is indicated by the yellow color. (F) A CPN with vacuoles. In (F') (a single optical section of the boxed area) the vacuoles marked with arrows contain small foci of KCC2+ and TGN38+ material (see animation along the Z axis in Supplementary File S3 and Supplementary Legends File). All are from 3 M *Tsc1CKO* mice. Confocal microscopy. Scale bars: A = 35 μm, B = 55 μm, C = 25 μm, D = 15 μm, D' = 8 μm, E = 25 μm, F = 15 μm.

from internalization of the surface protein, as has been found in seizures, after which the recycling vesicles can fuse with lysosomes or Golgi, although the vacuoles did not react with EEA1, an endosomal marker. Alternatively, the lack of plasma membrane KCC2 could result from a failure of membrane proteins to traffic to the plasma membrane in the first place.

The presence of vacuoles in the CPNs and the absence or weak staining of vacuolar membrane proteins in the cell plasma membrane suggests a problem with membrane trafficking. The activation of mTORC1 resulting from a loss of *Tsc1* or *Tsc2* leads to an inhibition of movement of membranes from the Golgi to the plasma membrane,[27,28] caused by abnormalities in microtubule protein transport, although this has not been analyzed in neurons. ER to Golgi trafficking may be enhanced, however.[29]

We found vacuoles of varying sizes in CPNs, suggesting an enlargement over time. A possible reason for the enlargement of vacuoles is the retention of proteins responsible for transmembrane ion transport (like KCC2 and Na+/K+-ATPase), which may lead to a redistribution of ions and their accumulation that creates a flux of osmotically-driven water and the consequent enlargement of vacuoles. The vacuoles appeared only in mice older than 3 M, following the development of seizures, and as noted above, seizures in combination with mTOR activation may be the inciting factor in the development of the vacuoles.

Cytoplasmic vacuoles are also present in the so-called "ballooned" cells or "giant cells" in tubers,[9] cells that have characteristics of undifferentiated or partially differentiated neuroectodermal cells.[30,31] These vacuolated giant cells appear

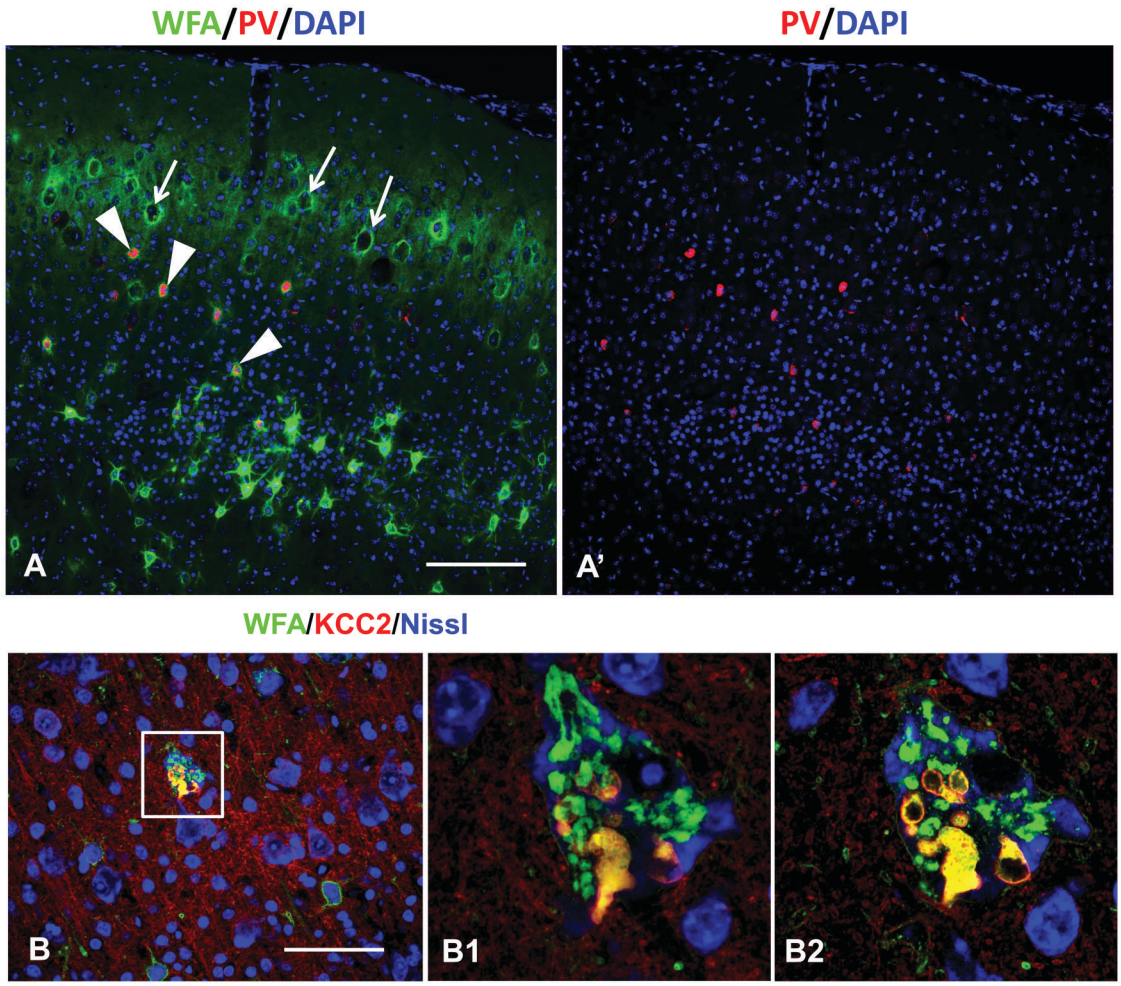

Figure 6. Unusual features of CPNs visualized with Wisteria floribunda agglutinin (WFA). (A) WFA is found on the plasma membranes of CPNs (arrows, only some marked) in addition to the normal expression on inhibitory neurons (arrowheads indicate parvalbumin [PV] immunopositive inhibitory neurons). (B) Intraneuronal vacuoles are stained with WFA. (B1) Enlarged boxed area in (B) shows CPN double stained for WFA and KCC2. Note that only some of the WFA immunopositive structures (in yellow) are KCC2+. (B2) A single optical section of the neuron shown in (D). 1.3 M *Tsc1CKO* mice. Confocal microscopy. Scale bars: A = 175 μm, B = 145 μm.

in a *nestin-Cre* murine model of TSC,[9] and marker studies and EM suggest that the vacuoles represent derivatives of the lysosomal system. In contrast, in the *Tsc1CKO* mouse, we report the vacuoles in neurons. We do not know at this point whether the molecular pathways and pathology underlying giant cell and neuronal vacuolations have any common mechanisms.

In addition to a problem in membrane trafficking and possible osmotic accumulation that enlarges vacuole size, could the presence of vacuoles in CPNs denote a condition that may lead to cell death? In non-neuronal cells, cytoplasmic vacuolization is often accompanied by cell death. Hence, the vacuoles we observed in CPNs may represent a sign of neuronal degeneration.[32]

CD44 is only found in mouse CPNs

The presence of CD44 in plasma membranes and in the cytoplasm is not typical for normal cortical neurons; although we found it in mouse CPNs, we did not find it in any normal-sized neurons, neither recombinant nor non-recombinant. It was not present in any neurons in human tubers and the neighboring cortex, including the cytomegalic neurons. CD44 has been reported in giant cells and in astrocytes in TSC.[5,33] It is thus likely that the upregulation of *CD44,* found at the transcriptional level[34] in human TSC, occurs in giant cells and astrocytes but not in neurons. The widespread expression of CD44 in neurons in the mouse TSC model may represent a species peculiarity of this pathology.

KCC2 is decreased in TSC and cortical dysplasias

A decrease in KCC2 in neuronal plasma membranes in TSC and mTOR-related cortical dysplasia is well documented.[24,35–37] The mechanisms responsible for such decrease are elusive, however. Here we propose a novel explanation based on abnormal intracellular trafficking and the retention of KCC2

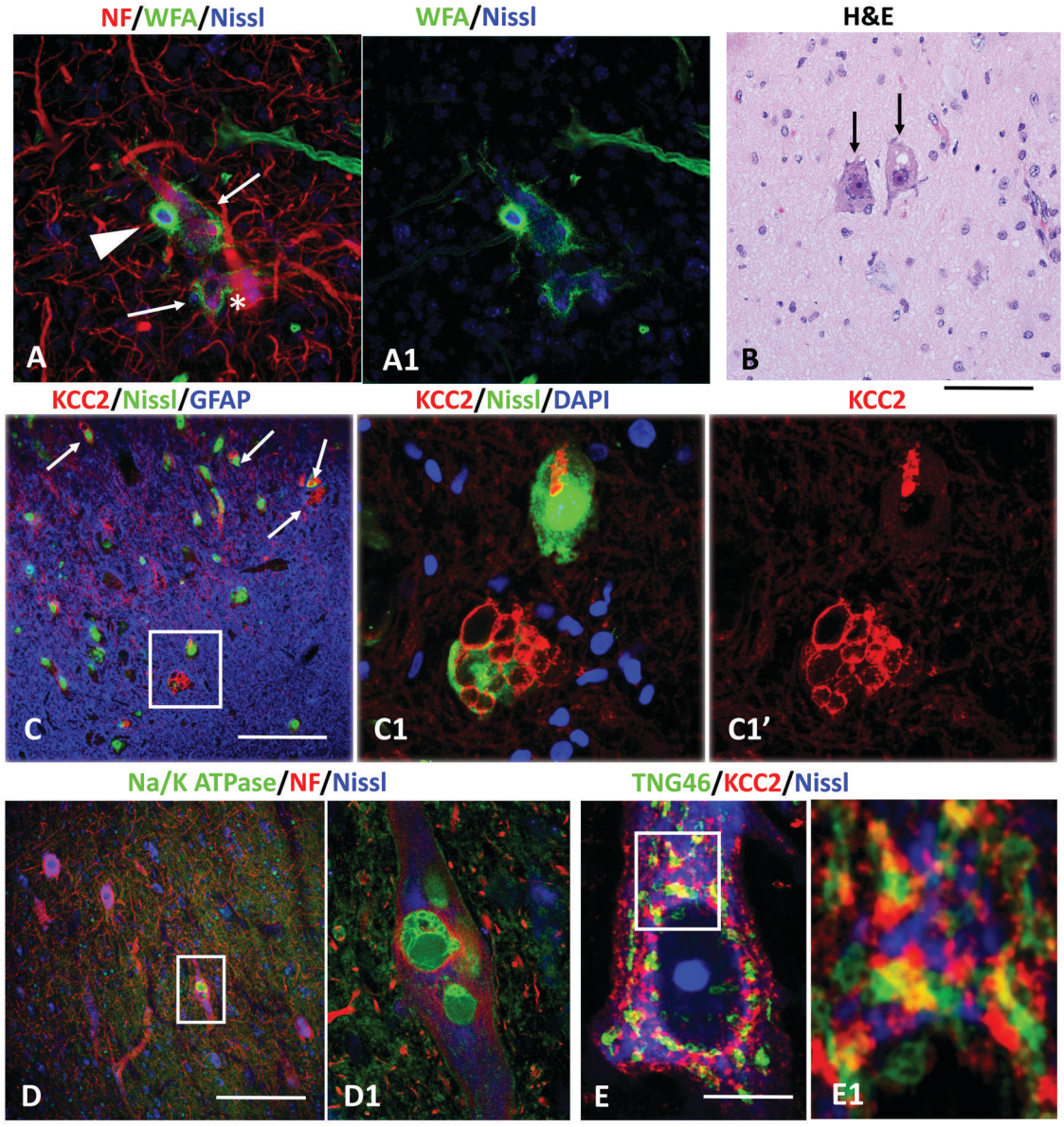

Figure 7. Abnormal features of cytomegalic neurons in cortical tubers in human tuberous sclerosis complex. (A) PNNs around cytomegalic neurons (arrows). Small neurons with perineuronal nets with high levels of Wisteria floribunda agglutinin (arrowhead) are probably inhibitory neurons. A cytomegalic neuron without a PNN is marked with an asterisk. (B) Two cytomegalic neurons with vacuoles (arrows). Hematoxylin and eosin-stained section. (C) Vacuoles immunolabeled with KCC2 (boxed area and arrows in C) in cytomegalic neurons. (C1) A single optical section of the enlarged boxed area in (C). (C1') Shows immunolabelling for KCC2 alone. Note that neurons with KCC2+ vacuoles have very weak KCC2 staining of the plasma membrane. (D) Na+/K+ ATPase in the vacuoles in cytomegalic neurons. (D1) Shows the enlarged boxed area in (D). (E) A cytomegalic neuron with diffusely distributed KCC2-immunopositive material, some profiles of which are colocalized with the Golgi marker, TGN46. Nissl in blue. (E1) Shows the enlarged boxed area in (E). Areas in yellow correspond to the colocalization of KCC2 and TNG46 (see animation along the Z-axis in Supplementary File S4 and Supplemental Legends File). Confocal microscopy. Scale bars: A = 40 µm, B = 55 µm, C = 65 µm, D = 60 µm, E = 20 µm.

in vacuoles associated with the Golgi complex. The nature of abnormal membrane trafficking from Golgi to the plasma membrane is an important subject for future investigation.

The PNNs are an abnormal pathology

Another pathological change was the appearance of PNNs around CPNs. This change was observed in the mouse TSC model and in the cytomegalic neurons in human cortical tubers. It is possible that, similar to what has been described in the CA2 hippocampal area,[38] PNNs around pyramidal neurons in the cortex predispose to seizures. This aberrant localization of PNNs around excitatory neurons in mice and humans is a novel feature of neuronal changes in TSC pathology.

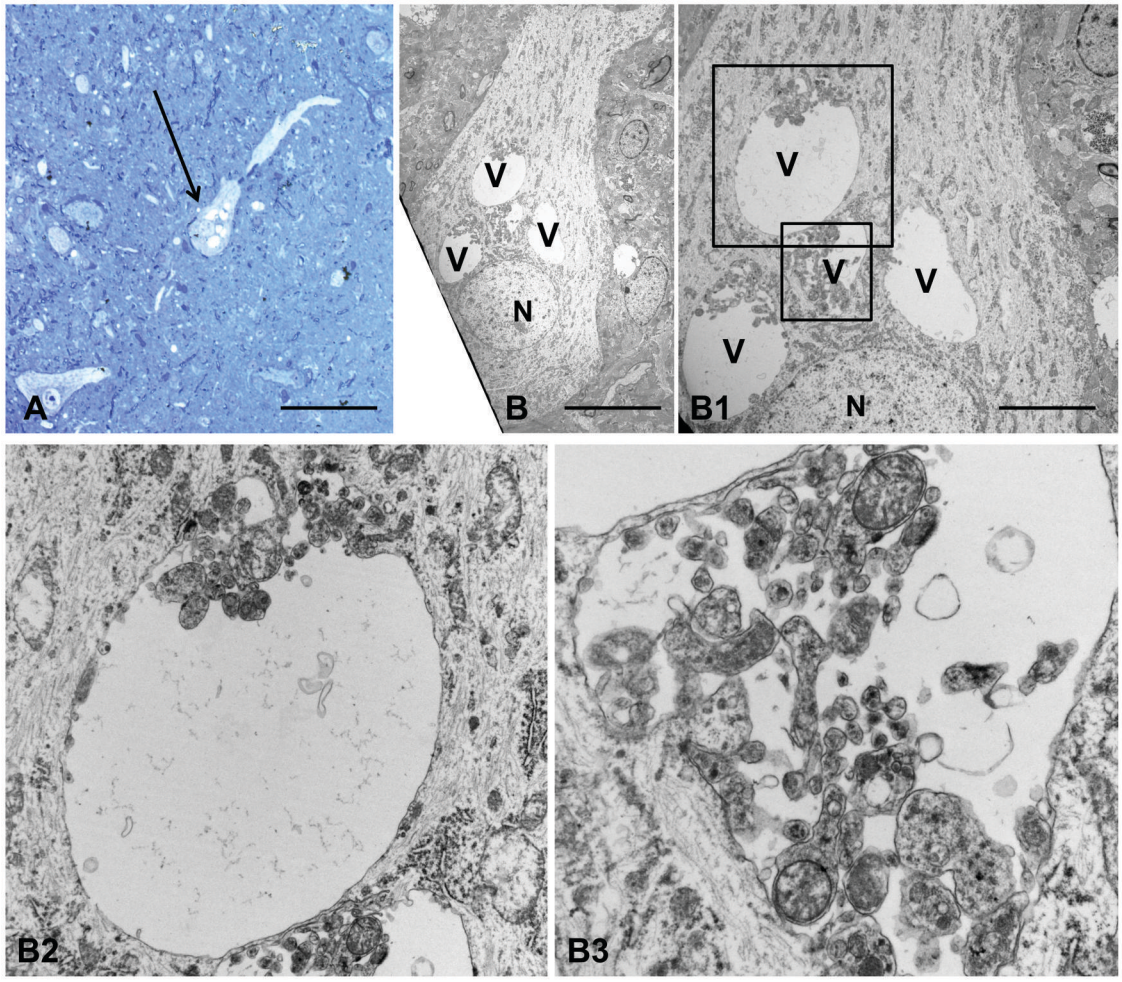

Figure 8. Ultrastructure of a cytomegalic neuron with vacuoles in a human cortical tuber. (A) Semi-thin section stained with toluidine blue. The neuron with vacuoles is marked with an arrow. (B) A cytomegalic neuron with several vacuoles [V]. The vacuoles contain different amounts of cytoplasmic inclusions and the ultrastructural organization of vacuoles is similar to that in the *Tsc1CKO* mice. (B1) Shows an enlarged central part of the neuron shown in (B). (B2) Shows the enlarged upper boxed area in (B1). (B3) Shows the enlarged lower boxed area in (B1). Scale bars: A = 95 μm, B = 8 μm, B1 = 15 μm.

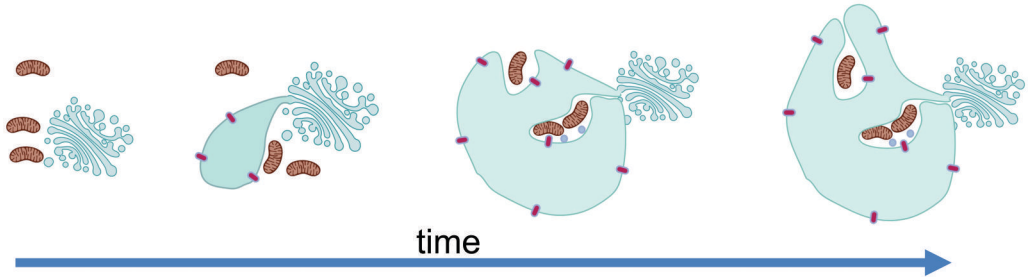

Figure 9. Schematic presentation of the possible development of vacuoles from the Golgi. From left to right: normal Golgi with surrounding mitochondria (brown); vacuole emanating from the Golgi, containing membrane molecules (like KCC2 and Na+/K+ ATPase pumps, shown in purple); larger vacuoles encircling cytoplasmic organelles (shown as enclosed mitochondria); gradual increase in vacuolar size due to the functioning of the ion pumps.

In conclusion: (1) Cytomegalic neurons in both a mouse TSC model and in human TSC have abnormal, cytoplasmic vacuoles that are likely a result of the failure of the normal trafficking of membrane molecules from the Golgi to the plasma membrane. (2) Cytomegalic neurons in both a mouse TSC model and in human TSC are abnormally surrounded by PNNs.

ACKNOWLEDGMENTS

Image processing and analysis was performed in the Confocal and Specialized Microscopy Shared Resource of the Herbert Irving Comprehensive Cancer Center at Columbia University, supported by NIH/NCI grant # P30CA013696.

SUPPLEMENTARY MATERIAL

Supplementary material is available at academic.oup.com/jnen.

FUNDING

J.E.G. was supported by DOD TSCRP Idea Development Award W81XWH-15-1-0112. G.M. was supported by K08-NS048064 (NIH/NINDS) and the Tuberous Sclerosis Alliance. G.T. was supported by DOD TSCRP Idea Development Awards W81XWH-16-1-0263, W81XWH-15-1-0112 and K01 MH096956 (NIH/NIMH).

CONFLICTS OF INTEREST

The authors have no conflicts of interest to declare.

DATA AVAILABILITY

There are no research data or data files other than the text and images presented in this article.

REFERENCES

1. Wong M, Crino PB. Tuberous sclerosis and epilepsy: role of astrocytes. *Glia*. 2012;60:1244-1250.
2. Hasbani DM, Crino PB. Tuberous sclerosis complex. *Handb Clin Neurol*. 2018;148:813-822.
3. Marcotte L, Aronica E, Baybis M, et al. Cytoarchitectural alterations are widespread in cerebral cortex in tuberous sclerosis complex. *Acta Neuropathol*. 2012;123:685-693.
4. Crino PB. Evolving neurobiology of tuberous sclerosis complex. *Acta Neuropathol*. 2013;125:317-332.
5. Sosunov AA, McGovern RA, Mikell CB, et al. Epileptogenic but MRI-normal perituberal tissue in Tuberous Sclerosis Complex contains tuber-specific abnormalities. *Acta Neuropathol Commun*. 2015;3:17.
6. Crino PB, Henske EP. New developments in the neurobiology of the tuberous sclerosis complex. *Neurology*. 1999;53:1384-1390.
7. Meikle L, Talos DM, Onda H, et al. A mouse model of tuberous sclerosis: neuronal loss of Tsc1 causes dysplastic and ectopic neurons, reduced myelination, seizure activity, and limited survival. *J Neurosci*. 2007;27:5546-5558.
8. Feliciano DM, Su T, Lopez J, et al. Single-cell Tsc1 knockout during corticogenesis generates tuber-like lesions and reduces seizure threshold in mice. *J Clin Invest*. 2011;121:1596-1607.
9. Goto J, Talos DM, Klein P, et al. Regulable neural progenitor-specific Tsc1 loss yields giant cells with organellar dysfunction in a model of tuberous sclerosis complex. *Proc Natl Acad Sci U S A*. 2011;108:E1070-1079.
10. Crowell B, Lee GH, Nikolaeva I, et al. Complex Neurological Phenotype in Mutant Mice Lacking Tsc2 in Excitatory Neurons of the Developing Forebrain. *eNeuro*. 2015;2:e0046-15.
11. Robens BK, Grote A, Pitsch J, et al. Minute amounts of hamartin wildtype rescue the emergence of tuber-like lesions in conditional Tsc1 ablated mice. *Neurobiol Dis*. 2016;95:134-144.
12. Zou J, Zhang B, Gutmann DH, et al. Postnatal reduction of tuberous sclerosis complex 1 expression in astrocytes and neurons causes seizures in an age-dependent manner. *Epilepsia*. 2017;58:2053-2063.
13. Kwon CH, Zhu X, Zhang J, Baker SJ. mTor is required for hypertrophy of Pten-deficient neuronal soma in vivo. *Proc Natl Acad Sci U S A*. 2003;100:12923-12928.
14. Zhou J, Blundell J, Ogawa S, et al. Pharmacological inhibition of mTORC1 suppresses anatomical, cellular, and behavioral abnormalities in neural-specific Pten knock-out mice. *J Neurosci*. 2009;29:1773-1783.
15. Ljungberg MC, Sunnen CN, Lugo JN, et al. Rapamycin suppresses seizures and neuronal hypertrophy in a mouse model of cortical dysplasia. *Dis Model Mech*. 2009;2:389-398.
16. Cuesto G, Enriquez-Barreto L, Caramés C, et al. Phosphoinositide-3-kinase activation controls synaptogenesis and spinogenesis in hippocampal neurons. *J Neurosci*. 2011;31:2721-2733.
17. Wu X, Sosunov AA, Lado W, et al. Synaptic hyperexcitability of cytomegalic pyramidal neurons contributes to epileptogenesis in tuberous sclerosis complex. *Cell Rep*. 2022;40:111085.
18. Weiner HL, Carlson C, Ridgway EB, et al. Epilepsy surgery in young children with tuberous sclerosis: results of a novel approach. *Pediatrics*. 2006;117:1494-1502.
19. Al-Dalahmah O, Sosunov AA, Sun Y, et al. The matrix receptor CD44 is present in astrocytes throughout the human central nervous system and accumulates in hypoxia and seizures. *Cells*. 2024;13:129.
20. Naruse M, Shibasaki K, Yokoyama S, et al. Dynamic changes of CD44 expression from progenitors to subpopulations of astrocytes and neurons in developing cerebellum. *PLoS One*. 2013;8:e53109.
21. Sawada R, Nakano-Doi A, Matsuyama T, Nakagomi N, Nakagomi T. CD44 expression in stem cells and niche microglia/macrophages following ischemic stroke. *Stem Cell Investig*. 2020;7:4.
22. Nakatogawa H. Mechanisms governing autophagosome biogenesis. *Nat Rev Mol Cell Biol*. 2020;21:439-458.
23. Alpar A, Gartner U, Hartig W, et al. Distribution of pyramidal cells associated with perineuronal nets in the neocortex of rat. *Brain Res*. 2006;1120:13-22.
24. Campbell SL, Robel S, Cuddapah VA, et al. GABAergic disinhibition and impaired KCC2 cotransporter activity underlie tumor-associated epilepsy. *Glia*. 2015;63:23-36.
25. Gonzalez MI. Regulation of the cell surface expression of chloride transporters during epileptogenesis. *Neurosci Lett*. 2016;628:213-218.
26. Chen L, Wan L, Wu Z, et al. KCC2 downregulation facilitates epileptic seizures. *Sci Rep*. 2017;7:156.
27. Jones KA, Jiang X, Yamamoto Y, et al. Tuberin is a component of lipid rafts and mediates caveolin-1 localization: role of TSC2 in post-Golgi transport. *Exp Cell Res*. 2004;295:512-524.
28. Jiang X, Yeung RS. Regulation of microtubule-dependent protein transport by the TSC2/mammalian target of rapamycin pathway. *Cancer Res*. 2006;66:5258-5269.
29. Koscielny A, Liszewska E, Machnicka K, et al. mTOR controls endoplasmic reticulum-Golgi apparatus trafficking of VSVg in specific cell types. *Cell Mol Biol Lett*. 2021;26:18.
30. Crino PB, Trojanowski JQ, Dichter MA, et al. Embryonic neuronal markers in tuberous sclerosis: single-cell molecular pathology. *Proc Natl Acad Sci U S A*. 1996;93:14152-14157.
31. Yamanouchi H, Jay V, Rutka JT, et al. Evidence of abnormal differentiation in giant cells of tuberous sclerosis. *Pediatr Neurol*. 1997;17:49-53.
32. Shubin AV, Demidyuk IV, Komissarov AA, et al. Cytoplasmic vacuolization in cell death and survival. *Oncotarget*. 2016;7:55863-55889.
33. Arai Y, Takashima S, Becker LE. CD44 expression in tuberous sclerosis. *Pathobiology*. 2000;68:87-92.

34. Boer K, Crino PB, Gorter JA, et al. Gene expression analysis of tuberous sclerosis complex cortical tubers reveals increased expression of adhesion and inflammatory factors. *Brain Pathol*. 2010;20:704-719.
35. Aronica E, Boer K, Redeker S, et al. Differential expression patterns of chloride transporters, Na+-K+-2Cl—cotransporter and K+-Cl—cotransporter, in epilepsy-associated malformations of cortical development. *Neuroscience*. 2007;145:185-196.
36. Talos DM, Sun H, Kosaras B, et al. Altered inhibition in tuberous sclerosis and type IIb cortical dysplasia. *Ann Neurol*. 2012;71:539-551.
37. Munakata M, Watanabe M, Otsuki T, et al. Altered distribution of KCC2 in cortical dysplasia in patients with intractable epilepsy. *Epilepsia*. 2007;48:837-844.
38. Carstens KE, Phillips ML, Pozzo-Miller L, et al. Perineuronal Nets Suppress Plasticity of Excitatory Synapses on CA2 Pyramidal Neurons. *J Neurosci*. 2016;36:6312-6320.

Journal of Neuropathology & Experimental Neurology, 2024, 00, 1–13
https://doi.org/10.1093/jnen/nlae079
Original Article